Monthly Notices of the ROYAL ASTRONOMICAL SOCIETY

MNRAS **469,** 4400–4413 (2017)
Advance Access publication 2017 May 15

doi:10.1093/mnras/stx1186

Detection of the Yarkovsky effect for C-type asteroids in the Veritas family

V. Carruba,[1,2]★ D. Vokrouhlický[3] and D. Nesvorný[2]

[1] *UNESP, Univ. Estadual Paulista, Grupo de dinâmica Orbital e Planetologia, Guaratinguetá, SP 12516-410, Brazil*
[2] *Department of Space Studies, Southwest Research Institute, Boulder, CO 80302, USA*
[3] *Institute of Astronomy, Charles University, V Holešovičkách 2, CZ-18000 Prague 8, Czech Republic*

Accepted 2017 May 11. Received 2017 May 11; in original form 2017 March 2

ABSTRACT

The age of a young asteroid family can be determined by tracking the orbits of family members backward in time and showing that they converge at some time in the past. Here we consider the Veritas family. We find that the membership of the Veritas family increased enormously since the last detailed analysis of the family. Using backward integration, we confirm the convergence of nodal longitudes Ω, and, for the first time, also obtain a simultaneous convergence of pericentre longitudes ϖ. The Veritas family is found to be $8.23^{+0.37}_{-0.31}$ Myr old. To obtain a tight convergence of Ω and ϖ, as expected from low ejection speeds of fragments, the Yarkovsky effect needs to be included in the modelling of the past orbital histories of Veritas family members. Using this method, we compute the Yarkovsky semimajor axis drift rates, $\mathrm{d}a/\mathrm{d}t$, for 274 member asteroids. The distribution of $\mathrm{d}a/\mathrm{d}t$ values is consistent with a population of C-type objects with low densities and low thermal conductivities. The accuracy of individual $\mathrm{d}a/\mathrm{d}t$ measurements is limited by the effect of close encounters of member asteroids to (1) Ceres and other massive asteroids, which cannot be evaluated with confidence.

Key words: celestial mechanics – minor planets, asteroids: general.

1 INTRODUCTION

Asteroid families are the outcomes of disruptive collisions of main belt asteroids. After a family-forming event, the orbits of fragments are affected by gravitational and non-gravitational forces, such as planetary perturbations and the Yarkovsky effect (Bottke et al. 2002; Vokrouhlický et al. 2015). The Yarkovsky effect acts to spread fragments in semimajor axis. It is therefore generally difficult, in the case of old asteroid families, to distinguish between the original spread caused by ejection velocities and the subsequent evolution by the Yarkovsky effect.

For young asteroid families (age <20 Myr), on the other hand, the semimajor axis spread is not affected by the Yarkovsky effect. Their orbital structure thus allows us to make inferences about the original ejection velocity field. This is why the young asteroid families are useful. In addition, by integrating the orbits of young family members backward in time and checking on the convergence of their longitudes of pericentre ϖ and node Ω, it is possible to determine the family's age (Nesvorný et al. 2003).

The Veritas family (Family Identification Number, FIN, 609; Nesvorný, Brož & Carruba 2015) was first studied by Milani & Farinella (1994). They found that the orbit of (490) Veritas diffuses chaotically in eccentricity due to a background mean motion resonance. For (490) Veritas to be classified as a member, the family must be young (<50 Myr; Milani & Farinella 1994). Subsequently, Nesvorný et al. (2003) used the convergence of Ω of Veritas members to determine that the family is only 8.3 Myr old. This very young age was linked to a spike in the terrestrial deposition of interplanetary dust particles at 8.2 ± 0.1 Myr ago (Farley et al. 2006).

Many asteroids have been discovered since 2003, and the population of Veritas members is now about 10 times larger than it was back then. Using techniques developed in Carruba, Nesvorný & Vokrouhlický (2016), here we investigate the interesting case of the Veritas family. Our goal is to: (i) revise the age estimate obtained in Nesvorný et al. (2003); (ii) show that the convergence constraint requires inclusion of the Yarkovsky effect in the backward integration; (iii) set constraints on values of the key parameters affecting the Yarkovsky force, such as the asteroids density and thermal conductivity and (iv) study the effect of close encounters with Ceres and other massive asteroids have had on the past orbital histories of family members.

The analysis of the Veritas family is complicated by the presence of the nearby 2:1 resonance with Jupiter, where the precession rate of the perihelion longitude, g, has a singularity. The precession rate g is therefore fast in the region of the Veritas family, which prevented Nesvorný et al. (2003) from demonstrating the convergence of ϖ. Here we were able to overcome this difficulty and obtain, for the first time, the simultaneous convergence of both Ω *and* ϖ. This increases

★ E-mail: vcarruba@feg.unesp.br

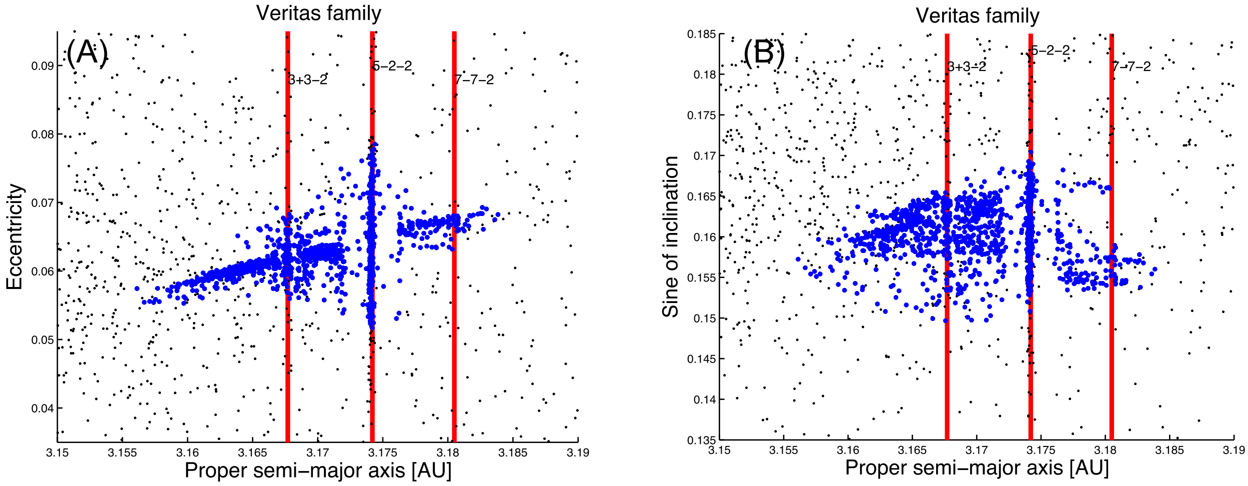

Figure 1. The (a, e) (panel A) and $(a, \sin i)$ (panel B) projections of orbits near the Veritas family. The vertical lines display the locations of main mean-motion resonances in the region. The blue symbols show the orbits of members of the Veritas family. The black dots display the background orbits.

our confidence that the present analysis correctly estimates the age of the Veritas family and constrains the principal parameters of the Yarkovsky effect.

2 FAMILY IDENTIFICATION AND DYNAMICAL PROPERTIES

As a first step of our analysis, we obtained the membership of the Veritas family from Nesvorný et al. (2015), where the family was defined using the hierarchical clustering method (HCM; Bendjoya & Zappalà 2002) and a cut-off of 30 m s^{-1}. 1294 members of the Veritas family were identified in that work. Following Carruba & Nesvorný (2016) we identified objects in the local background of the Veritas family. For this, we used the data base of synthetic proper elements available at the AstDyS site (http://hamilton.dm.unipi.it/astdys; Knežević & Milani 2003, accessed on 2016 September 3). Asteroids were considered to belong to the local background if they had proper e and $\sin i$ near the Veritas family, namely $0.035 < e < 0.095$ and $0.135 < \sin i < 0.185$ (these ranges correspond to four standard deviations of the observed distribution of the Veritas family).

The values of proper a were chosen from the maximum and minimum values of Veritas members ±0.02 au, the averaged expected orbital mobility potentially caused by close encounters with massive asteroids over 4 Gyr (Carruba et al. 2013). Namely, this corresponds to an interval $3.15 < a < 3.19$ au. Overall, we found 2166 background asteroids. No other important dynamical groups can be found in the local background of the Veritas family (Carruba 2013). After removing members of the Veritas family, the local background consists of 872 asteroids. The Veritas family and its background are shown in Fig. 1.

Chaotic dynamics in the region of the Veritas family was studied in detail in Milani & Farinella (1994) and Tsiganis, Knežević & Varvoglis (2007). Interested readers can find more information in those papers. Here we just consider the information about Veritas family members that can be obtained from their Lyapunov times. Tsiganis et al. (2007) identified two main chaotic regions in the Veritas family: one, with Lyapunov times $<3 \times 10^4$ yr, associated with the three-body resonance 5-2-2 (or 5J:-2S:-2A in alternative notation) and its multiplet structure, and another one, with $3 \times 10^4 < T_{\rm L} < 10^5$ yr, caused by the interaction of asteroids with the 3+3-2 resonance (or 3J:3S:-2A). Another three-body resonance identified in the region was the 7-7-2 resonance, but that only affected a single asteroid [(37005) 2000 TO37].

Objects with Lyapunov times longer than 10^5 yr and semimajor axes lower than that of the 3+3-2 resonance were classified as R_1 objects, while regular asteroids between the 3+3-2 and 5-2-2 resonances were classified as R_2 asteroids (Tsiganis et al. 2007). Only one regular Veritas family member was known with semimajor axis larger than that of the 5-2-2 resonance. A significant population of objects in this region is, however, currently known (139 asteroids, Fig. 1). Extending the notation from Tsiganis et al. (2007), we define these asteroids as R_3 objects.

Concerning secular resonances in the region of the Veritas family, an extensive study of the secular dynamics was performed in Carruba (2013) and Carruba et al. (2014). The two main secular resonances near the Veritas family are the $g - 2g_6 + g_5 + s - s_7$ (or, in terms of the linear secular resonances arguments, $2\nu_6 - \nu_5 + \nu_{17}$) and $g - g_6 + 2s - 2s_6$ (or $\nu_6 + 2\nu_{16}$) resonances. Only 10 outer main belt asteroids were found to librate in these resonances. They do not thus play a significant role in the dynamical evolution of the Veritas family.

Fig. 2 shows the (a, e) projection of asteroids near the Veritas family. The colour code identifies the degree of chaoticity associated with a given orbit: regular orbits are shown as black dots, orbits with $3 \times 10^4 < T_{\rm L} < 10^5$ yr are shown as green full circles and orbits with $T_{\rm L} < 3 \times 10^4$ yr are shown as blue full circles. With the exception of the new population of regular objects beyond the 5-2-2 resonance, our analysis essentially confirms that of Tsiganis et al. (2007).

3 PHYSICAL PROPERTIES

A detailed analysis of physical properties of asteroids in the region of the Themis, Hygiea and Veritas families was reported in Carruba (2013). Here we briefly summarize the physical properties of asteroids near the Veritas family. There are 146 objects with photometric data in the Sloan Digital Sky Survey-Moving Object Catalog 4 (SDSS-MOC4) data (Ivezić et al. 2001) in this region, 89 of which (61 per cent of the total) are members of the Veritas family. In addition, 784 objects have geometric albedo and absolute magnitude information available in the *Wide-field Infrared Survey*

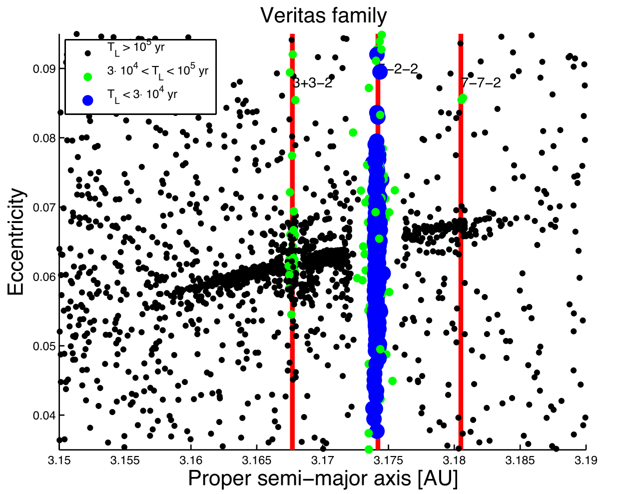

Figure 2. The (a, e) projection of orbits in the local background of the Veritas family. Objects with Lyapunov times $T_{\rm L} > 10^5$ yr are shown as black dots, objects with $3 \times 10^4 < T_{\rm L} < 10^5$ yr are displayed as green full circles and objects with $T_{\rm L} < 3 \times 10^4$ yr are shown as blue full circles. The Lyapunov times were obtained from the AstDyS catalogue (Knežević & Milani 2003).

Explorer (*WISE*) and *Near-Earth Object Wide-field Infrared Survey Explorer* (*NEOWISE*) data bases (Masiero et al. 2012).

Fig. 3 shows the taxonomic classification of asteroids obtained from SDSS-MOC4 with the method of DeMeo & Carry (2013) (panel A), and the *WISE* geometric albedo p_V (panel B). In panel (B), we separate dark asteroids (compatible with the C-complex taxonomy; $p_V < 0.12$) and bright asteroids (S-complex taxonomy; $0.12 < p_V < 0.30$; Masiero et al. 2012). The Veritas family is obviously a C-type family, and the C-complex objects also dominate the local background. In total, we found 97 Cs, 39 Xs and 3 Ds in the region, all belonging to the C-complex. There were only seven S-complex asteroids, four of which are S-type, two K-type and one A-type. The proportion of C- and S-complex asteroids is consistent with the available geometric albedo data: of the 784 objects with *WISE* albedo, 715 (91.2 per cent of the total) have $p_V < 0.12$, and are compatible with a C-complex taxonomy.

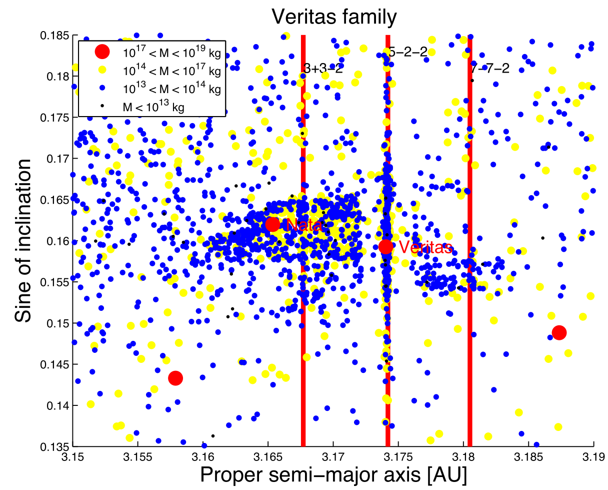

Figure 4. An (a, sin i) projection of asteroids near the orbital location of the Veritas family. The colour and size of the symbols reflect the estimated asteroid mass.

Finally, we estimated the masses of asteroids in and near the Veritas family assuming objects to be spherical with bulk density equal to 1300 kg m^{-3} (typical value of C-type objects). For objects with available *WISE* albedo data, we used the *WISE* p_V value to estimate their radius from the absolute magnitude (equation 1 in Carruba et al. 2003). For all other objects we used $p_V = 0.07$, which is the mean value of the Veritas family.

Fig. 4 shows our results. Among the Veritas members, only (490) Veritas and (1086) Nata have estimated masses larger than 10^{17} kg and diameters $D > 50$ km ($D = 110$ and 70 km, respectively). Smoothed particle hydrodynamics (SPH) simulation of the catastrophic disruption event that produced the Veritas family (Michel et al. 2011) indicates the observed size distribution of family members cannot be well reproduced if both (490) Veritas and (1086) Nata are true members of the family. Our analysis of the past convergence described in the following sections shows that the convergence of (1086) Nata can be demonstrated, while that of (490) Veritas cannot (because of the chaotic orbit of (490) Veritas). While it is not possible at this stage to positively decide whether (490) Veritas is

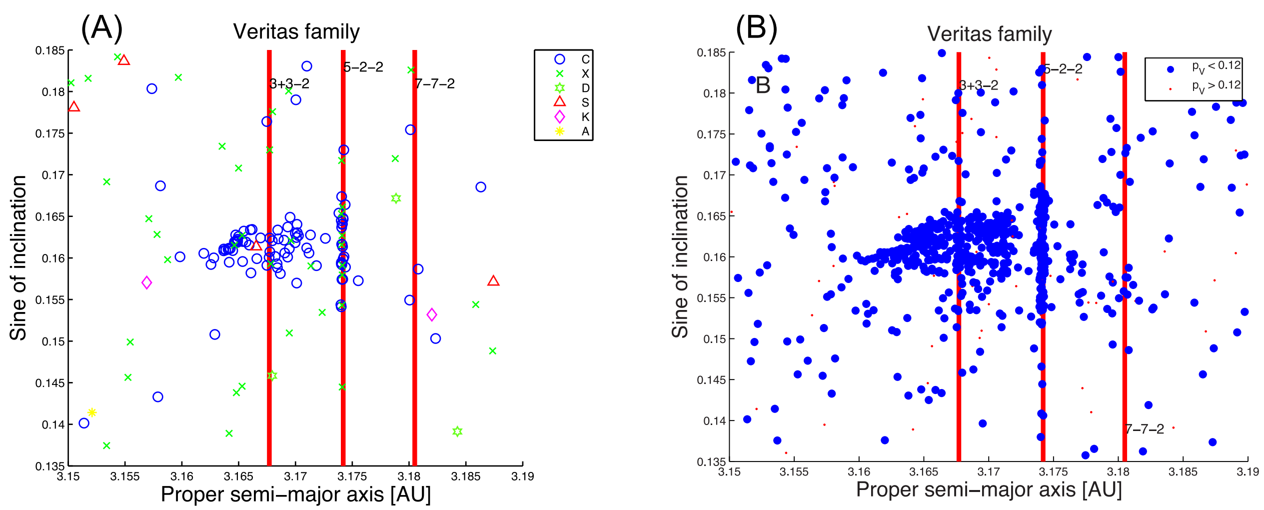

Figure 3. An (a, sin i) distribution of Veritas family asteroids, with taxonomic information (panel A) and *WISE* albedo data (panel B). Symbols used to identify asteroids with different spectral types and albedo values are identified in the inset.

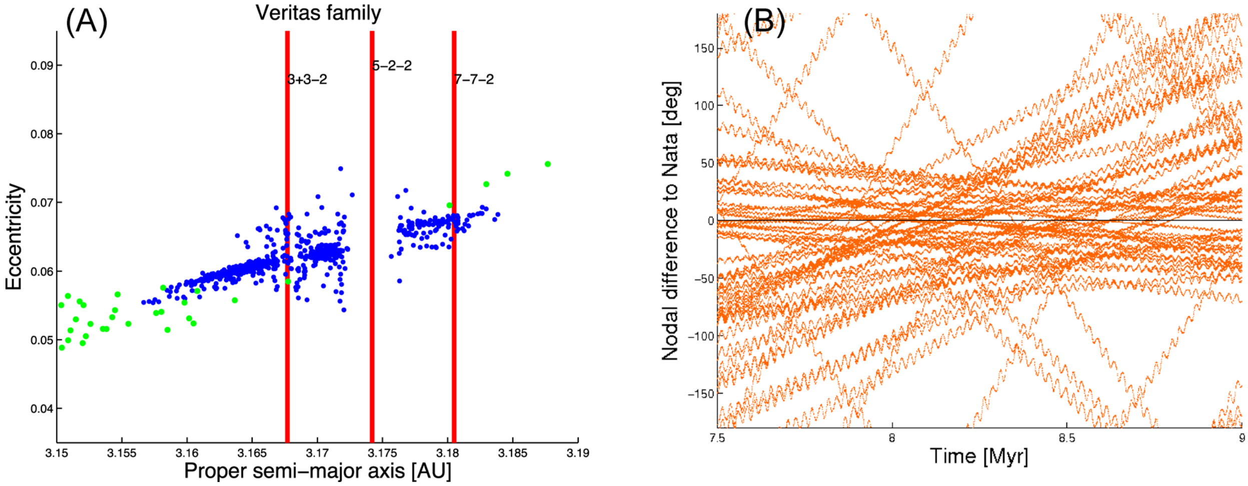

Figure 5. Panel (A): an (a, e) projection of Veritas family members (blue full circles) and background asteroids (green full circles) that passed our convergence criterion. Panel (B): convergence of the nodal longitudes at $\simeq$8.3 Myr of the first 50 members of the Veritas family (other members not shown for clarity). The vertical dashed lines display the approximate limits of the Veritas family age.

a member or not of its namesake family, for the purpose of our research we will use the orbit of (1086) Nata as a reference for the method of convergence of secular angles hereafter. Finally, since the combined volume of the Veritas members, barring (490) Veritas itself, is about 40 per cent of the total volume of the family, the family-forming event should be characterized as a catastrophic disruption.

4 PAST CONVERGENCE OF THE NODAL LONGITUDES

Following the approach described in Nesvorný et al. (2003), Nesvorný & Bottke (2004) and Carruba et al. (2016) for the Veritas and Karin families, we checked for a past convergence of orbits of members of the Veritas family and objects in the local background. We first focus on demonstrating the convergence of Ω, because the convergence of ϖ is complicated by the proximity to the 2:1 resonance (both the g frequency and its derivative, $\partial g/\partial a$, are large; Nesvorný et al. 2003).

To start with, to avoid strongly chaotic orbits, we selected 918 members of the Veritas dynamical family with $T_L > 3 \times 10^4$ yr. The chaotic orbits are mostly found in the identified three-body resonances and we cannot use them because their orbital histories cannot be computed deterministically. The selected orbits were integrated backward in time with SWIFT_MVSF, which is a symplectic integrator programmed by Levison & Duncan (1994). It was modified by Brož (1999) to include online filtering of the osculating elements. All eight planets were included in the integration as massive perturbers. We used a time step of 1 d. The Yarkovsky effect was not included in this initial integration.

Using the approach described in Carruba et al. (2016), we first checked for the past convergence of Ω. Asteroid (1086) Nata was used as a reference body, because its orbit has very long Lyapunov time [(490) Veritas cannot be used for this purpose because its orbit in the 5-2-2 resonance is strongly chaotic]. Specifically, we required that Ω of individual orbits converge to within $\pm 60°$ about Nata's Ω in the time interval between 8.1 and 8.5 Myr ago, which encompasses the age of the Veritas family estimated in Nesvorný et al. (2003). Out of the 918 considered bodies, 705 (76.8 per cent of the total) passed this test.

We then turned our attention to objects in the Veritas family background. First, as in Carruba et al. (2016), we computed the terminal ejection velocities for the 705 bodies that passed the above criterion by inverting Gauss equations (Murray & Dermott 1999):

$$\frac{\delta a}{a} = \frac{2}{na(1-e^2)^{1/2}}[(1+e\cos f)\delta v_t + e\sin f\,\delta v_r], \tag{1}$$

$$\delta e = \frac{(1-e^2)^{1/2}}{na}\left[\frac{e+2\cos f+e\cos^2 f}{1+e\cos f}\delta v_t + \sin f\,\delta v_r\right], \tag{2}$$

$$\delta i = \frac{(1-e^2)^{1/2}}{na}\frac{\cos(\omega+f)}{1+e\cos f}\delta v_W, \tag{3}$$

where $\delta a = a - a_{ref}$, $\delta e = e - e_{ref}$, $\delta i = i - i_{ref}$, a_{ref}, e_{ref} and i_{ref} define a reference orbit (we set $a_{ref} = 3.170$ au, $e_{ref} = 0.062$ and $i_{ref} = 9.207°$) and f and ω are the true anomaly and perihelion argument of the disrupted body at the time of impact. As in Tsiganis et al. (2007), we used $f = 30°$ and $\omega + f = 180°$.

The highest terminal ejection velocities observed inferred from this exercise, excluding objects that obviously drifted away in the three-body resonances, was 200 m s^{-1}. We then integrated backward in time asteroids in the local background of the Veritas family as defined in Section 2 and eliminated objects that (i) had Lyapunov times shorter than 3×10^4 yr and (ii) had ejection velocities with respect to the reference orbit larger than 220 m s^{-1} (i.e. 10 per cent larger than the maximum value determined above) and (iii) did not show the convergence of Ω to within $\pm 60°$ around that of (1086) Nata between 8.1 and 8.5 Myr ago.

Only 31 asteroids satisfied these requirements. Since, however, most of these objects were located at semimajor axis significantly smaller than those of the HCM members of the Veritas family (Fig. 5, panel A), we decided not to consider them for the following analysis. After eliminating taxonomical interlopers, we were left with 704 members of the Veritas family. Fig. 5, panel (A), shows the orbits of 704 members. Panel (B) of that figure illustrates the convergence of nodal longitudes at $\simeq$8.3 Myr ago.

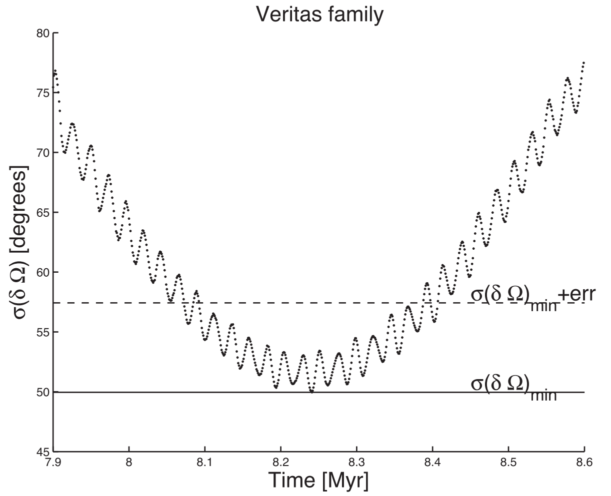

Figure 6. The evolution of the standard deviation of $\Delta\Omega$ as a function of time. The horizontal line identifies the minimum value of $\Delta\Omega$, while the dashed line shows the minimum value plus its error, assumed equal to one standard deviation of the $\Delta\Omega$ values over the length of our integration.

5 FAMILY AGE AND DETECTION OF THE YARKOVSKY EFFECT

The next step of our analysis is to obtain a preliminary estimate of the age of the Veritas family (as done in Carruba et al. 2016 for the Karin cluster), and show the necessity to include the Yarkovsky effect in the backward integration in order to improve the convergence. We do this numerically. The maximum Yarkovsky drift in a for a 2-km C-type object, the smallest body in our Veritas sample, is roughly 2.0×10^{-3} au over 8.3 Myr (see Brož et al. 2013 and Section 7). For each of the 704 members of the Veritas family we therefore created 11 clones with the same initial orbits. Each clone was assigned a drift rate, $\mathrm{d}a/\mathrm{d}t$, from -3.0×10^{-10} to 3.0×10^{-10} au yr^{-1}, with a step of 0.6×10^{-10} au yr^{-1} between individual clones.

The limits of $\mathrm{d}a/\mathrm{d}t$ correspond to the maximum negative and positive total drifts of 2.5×10^{-3} au, i.e. about 25 per cent larger than the maximum expected change in a for the smallest fragment over the estimated age of the family. All 7744 clones were then integrated backward in time over 10 Myr with SWIFT_RMVS3_DA, a symplectic integrator based on SWIFT_RMVS3 code (Levison & Duncan 1994) that was modified by Nesvorný & Bottke (2004) to include a constant drift in the semimajor axis.

The integration was used to refine the age estimate of the Veritas family. Here we only used the past convergence of Ω. For each time output of the integration between 7.9 and 8.6 Myr ago, we computed the standard deviation of $\Delta\Omega$ values [δs computed with respect to (1086) Nata] for 704 clones of our simulation with *zero* Yarkovsky drift. We then searched for the minimum of the standard deviation of $\Delta\Omega$. Fig. 6 displays the time evolution of $\sigma(\Delta\Omega)$ as a function of time for the simulated asteroids. Based on this, the age of the Veritas family was found to be 8.24 ± 0.17 Myr.

Adopting this age, we identified the value of $\mathrm{d}a$ for each clone that minimizes its $\Delta\Omega$. We found that the convergence in $\Delta\Omega$ is still not perfect, partly because of the rough resolution of $\mathrm{d}a/\mathrm{d}t$ with only 11 clones and partly because many near resonant orbits, which were not filtered out with our Lyapunov time cut, displayed significant chaos. To avoid these problems, we applied a narrower selection of 274 objects, which (i) have semimajor axes less than 3.166 au (to avoid possible interactions with the 3+3-2 resonance) and (ii) have Lyapunov times greater than 2×10^5 yr, to avoid chaotic orbits. Since one of our goals with this numerical experiment is to verify the possible past convergence of ϖ, we believe that our approach based on selecting the most regular objects in the R_1 region, including (1086) Nata, is justified. For each value of $\mathrm{d}a/\mathrm{d}t$ obtained from the previous simulations, we created 31 additional clones of the same particle with $\mathrm{d}a/\mathrm{d}t$ values covering plus or minus the step value of 0.6×10^{-10} au yr^{-1} used in the previous integration. Overall, we integrated 8494 orbits.

To better identify the orbits whose ϖ angles converge to that of (1086) Nata, we filtered $\Delta\Omega_i = \Omega_i - \Omega_{\mathrm{Nata}}$ and $\Delta\varpi_i = \varpi_i - \varpi_{\mathrm{Nata}}$, where the subscript i indicates the ith asteroid, with a low-pass digital Fourier filter (see Carruba 2010 for a description of the filtering method). This removed all frequency terms with periods shorter than 10^5 yr. Fig. 7 illustrates this procedure in an example.

We then analysed the time behaviour of the digitally filtered $\Delta\Omega$ and $\Delta\varpi$ angles. We first obtained a refined age estimate of the Veritas family using two approaches: for each of the 31 clones of a given asteroid, we selected the one with the minimum values of

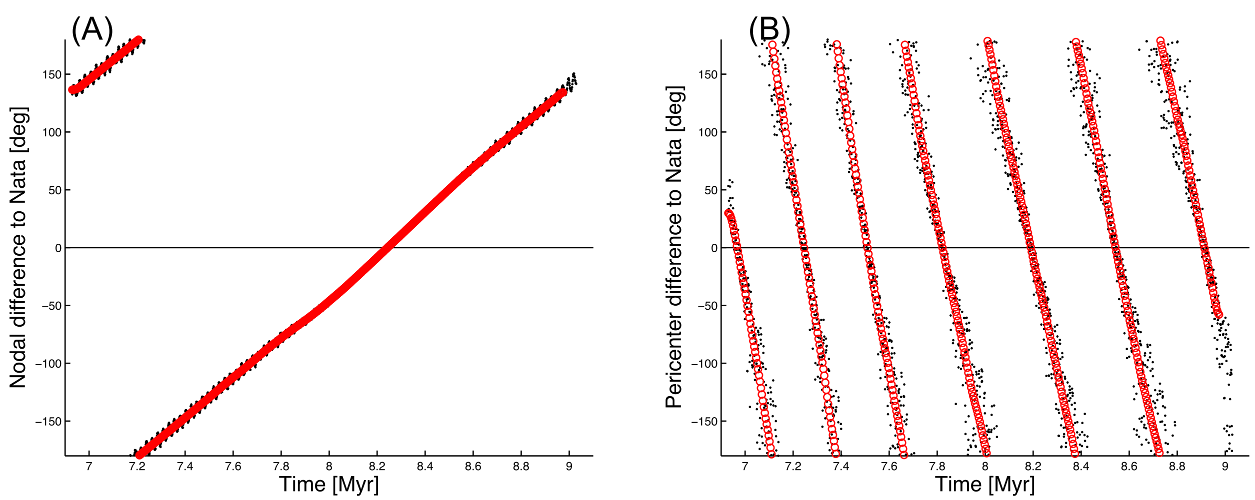

Figure 7. Osculating (black dots) and filtered (red circles) values of $\Delta\Omega = \Omega_{\mathrm{ast}} - \Omega_{\mathrm{Nata}}$ (panel A), and of $\Delta\varpi = \varpi_{\mathrm{ast}} - \varpi_{\mathrm{Nata}}$ (panel B), for one of the 8494 integrated particles in the second run. All frequency terms with a period smaller than 10^5 yr were removed in the filtered elements.

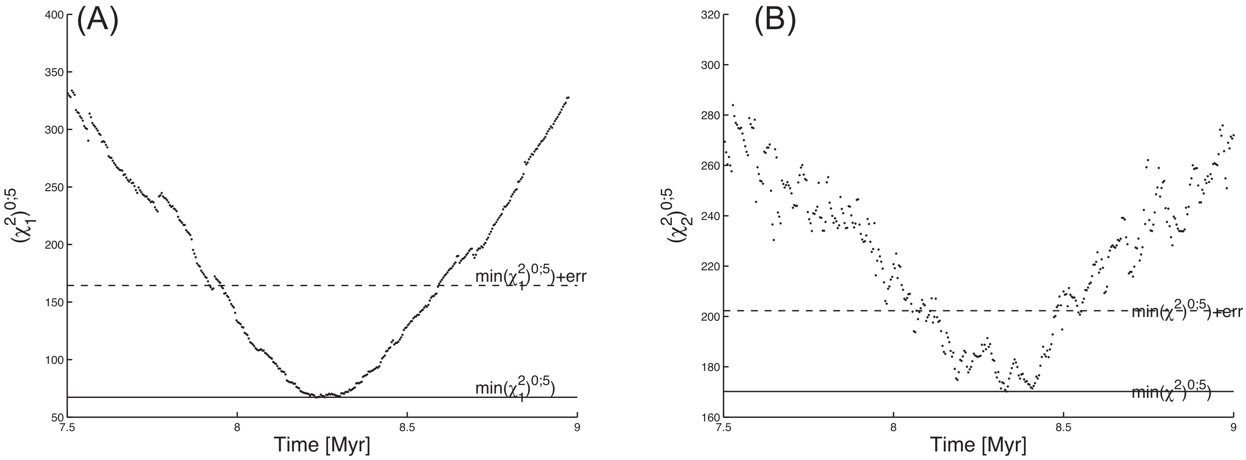

Figure 8. Time evolution of the square root of χ^2, as defined in equations (4) and (5). The horizontal black line displays the minimum value of these quantities, while the dashed line shows the minimum plus the error, defined as square root of the standard deviation of χ^2 over the considered time interval.

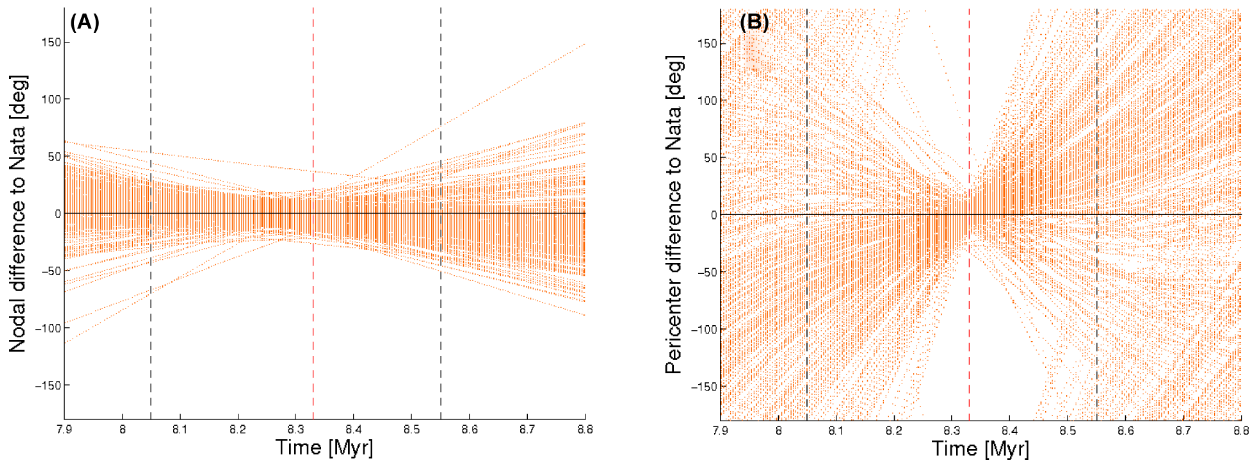

Figure 9. Convergence of filtered $\Delta\Omega$ (panel A) and $\Delta\varpi$ (panel B) for the 274 particles with the lowest values of these angles at the nominal family age. Vertical red line displays the nominal Veritas family age, while the vertical black dashed lines show the possible range of family ages obtained with the χ^2-like approach of equation (5).

$\Delta\Omega$ and $\Delta\varpi$ at each time step. We then computed χ^2-like variables using the relationships:

$$\chi_1^2 = \sum_{i=1}^{N_{\rm ast}} (\Delta\Omega_i)^2, \quad (4)$$

$$\chi_2^2 = \sum_{i=1}^{N_{\rm ast}} [(\Delta\varpi_i)^2 + (\Delta\Omega_i)^2], \quad (5)$$

where $N_{\rm ast} = 274$ is the number of asteroids in our sample. The first relationship will minimize the dispersion in $\Delta\Omega$, while the second will minimize the dispersion in both $\Delta\Omega$ and $\Delta\varpi$. Since the convergence in $\Delta\Omega$ is more robust, the first method provides a better estimate for the age. We will consistently use results from this first method hereafter. The second method, however, shows that convergence in $\Delta\varpi$ is actually possible, at least in the numerical model here considered.

Fig. 8 displays the time evolution of the square root of these two quantities (see panels A and B). We define the nominal error of $\sqrt{\chi^2}$ as the standard deviation of these quantities over the considered time interval. Based on this analysis, the Veritas family is $8.23^{+0.37}_{-0.31}$ Myr old. It is important to point out that, for the first time, we were also able to obtain the convergence of ϖ. At the nominal family age of $8.33^{+0.22}_{-0.28}$ Myr obtained with the second method, we identified a set of 274 clones whose angles have minimum values of $\Delta\varpi$ and $\Delta\Omega$. The result is shown in Fig. 9: the age solutions of the Veritas family with both methods are statistically identical. Apart from internal consistency, it also justifies the convergence of the longitudes of pericentre. Overall, the convergence of the angles is remarkable: the standard deviations of the distribution in $\Delta\Omega$ and $\Delta\varpi$ at the family nominal age are 8°.4 and 8°.7, respectively. Fig. 10 shows histograms of the two distributions. The results obtained with the first method were similar: the standard deviations in this case are equal to 7°.7 and 8°.9, respectively.

As the next step, we extracted the semimajor axis drifts d*a* from clones that show the best convergence at the nominal family age. The result is shown in Fig. 11. We also obtained d*a* values at the limits of the age range (7.9 and 8.6 Myr). The distribution of d*a* values is similar in all these cases. As expected from the standard theory on the Yarkovsky effect, the larger asteroids have smaller d*a* values. We discuss this in more detail in Sections 7 and 8. A

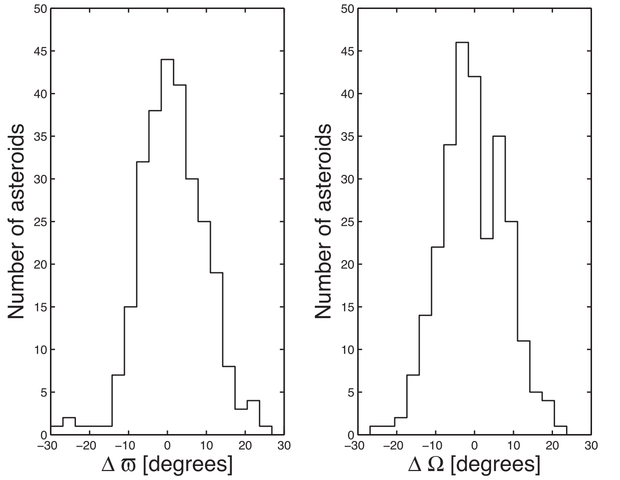

Figure 10. Histograms of the distributions of $\Delta\varpi$ and $\Delta\Omega$ obtained at the family nominal age of 8.33 Myr, computed with our second approach.

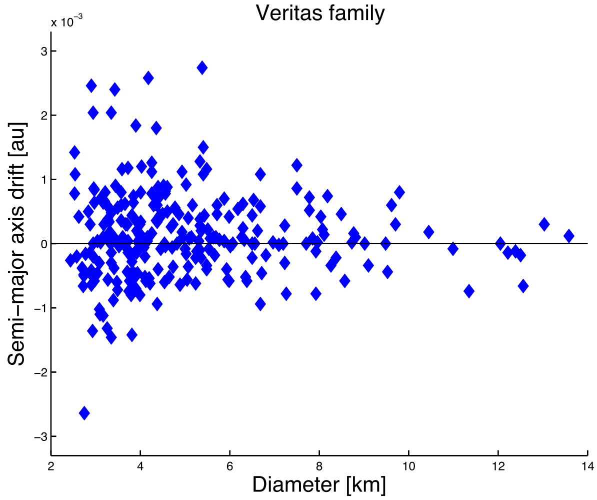

Figure 11. Semimajor axis drift da of Veritas family members over the estimated age of the Veritas family (8.23 Myr). The drifts tend to be smaller for larger members, as expected from the size dependency of the Yarkovsky effect.

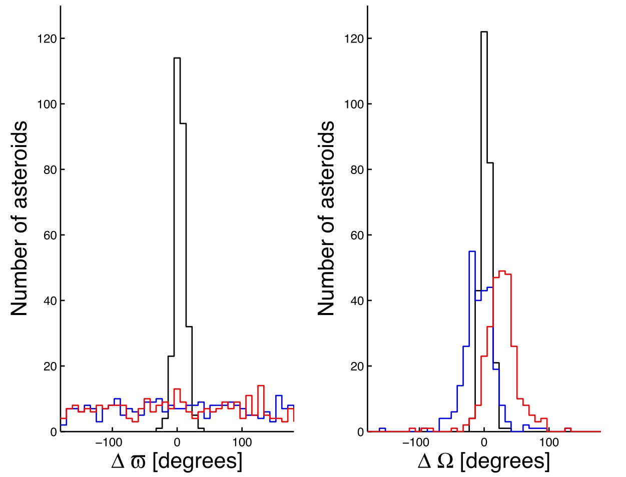

Figure 12. Distribution of changes in ϖ and Ω for the 274 integrated asteroids for the case without Ceres and Hygiea (black line), with Ceres (blue line) and with Ceres and Hygiea (red line).

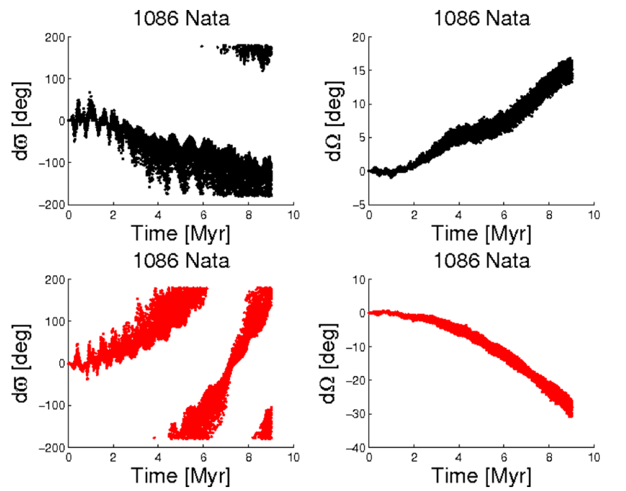

Figure 13. $\Delta\varpi$ and $\Delta\Omega$ values as a function of time for (1086) Nata when Ceres was considered as a massive perturber (top panels, black dots) and when Ceres and Hygiea were both considered as perturbers (bottom panels, red dots). The values were computed relative to a reference case where no massive asteroid perturbers were included in the integration.

list of the 274 studied asteroids with their proper elements a, e, $\sin i$, proper frequencies g and s, Lyapunov exponents LCE and estimated drift speeds da/dt is given in Table B1, available in its full length in the electronic version of the paper.

6 EFFECTS OF ENCOUNTERS WITH (1) CERES AND (10) HYGIEA

To evaluate the effect that close encounters with massive main belt asteroids may have had on the convergence of the secular angles, we repeated the integration of our selected 274 Veritas members, but this time we also included the gravitational effect of (i) (1) Ceres and (ii) both (1) Ceres and (10) Hygiea. The latter asteroid, the fourth most massive in the main belt, was included because of its orbital proximity to the Veritas family and the possible role that the $g - g_{\rm Hygiea}$ secular resonance (see Appendix A for a discussion of the possible effect of this resonance).

Fig. 12 shows the distribution of changes of ϖ and Ω in different cases. The da values from the Yarkovsky effect were kept constant in all the three cases. In principle, fine tuning of these values, as performed in the previous section, could compensate the effects of encounters with Ceres and Hygiea, but, since the occurrence of a given encounter with a massive body at a given time depends on the Solar system model used (Carruba et al. 2012), adding more massive bodies to the simulations would require a different fine tuning.

Encounters with Ceres and Ceres/Hygiea increase the standard deviation of the distribution in $\Delta\Omega$ from 8°.4 up to 26°.2 and 26°.0, respectively. Surprisingly, they completely destroy the convergence in $\Delta\varpi$. Both models cause the standard deviation of the distribution in $\Delta\varpi$ to reach values near 101°.3, corresponding to a uniform distribution. What is causing this remarkable behaviour?

Fig. 13 shows values of $\Delta\varpi$ and $\Delta\Omega$ values as a function of time for (1086) Nata with respect to a reference case where no massive asteroids were included in the integration. It can be noted that while changes in $\Delta\Omega$ are smaller than 30° in both models, changes in $\Delta\varpi$ are bigger than 180° in the first model, and two complete circulations of this angle were observed in the second model. We can also observe that the time behaviour of the angles is different in the two models. While $\Delta\varpi$ increases in the first model, it decreases in the second one (and vice versa for $\Delta\Omega$).

Let us now try to understand what makes the secular angle convergence in the Veritas family so sensitive to gravitational perturbations of massive asteroids, and what it implies for the realistic uncertainty in our determination of the drift rates caused by the Yarkovsky effect. Our method is as follows.

The massive asteroids may affect the nominal convergence of secular angles in two ways: (i) a direct contribution to the secular frequencies s (node) and g (pericentre) or (ii) an indirect effect, which consists of perturbations of the semimajor axis a, being then reflected in nodes and pericentres via dependence of s and g on a. We believe the latter is dominant, and we will try to demonstrate it in the case of Ceres' influence. Obviously, the effect is larger in the longitude of pericentre just because the gradient $\partial g/\partial a$ is nearly an order of magnitude larger than $\partial s/\partial a$ in the Veritas family (see e.g. Appendix A).

We postulate that the nature of Ceres' perturbation in semimajor axis of Veritas orbits is due to stochastic jumps during sufficiently close encounters. These are favoured by two facts: (i) the orbit pericentre q for Veritas orbits is close to the orbit apocentre Q of Ceres, and (ii) the mean inclination of Veritas orbits is nearly the same as the mean inclination of Ceres' orbit. To probe how (i) and (ii) influence circumstances of close encounters to Ceres, we used the Öpik theory to compute intrinsic collision probability $p_{\rm i}$ of the two orbits. Indeed, we obtained $p_{\rm i} \simeq 3.5 \times 10^{-17}$ km^{-2} yr^{-1}, which is slightly larger than the average in the main belt (e.g. Bottke et al. 1994).

Given the difference of s frequencies of Veritas members and Ceres, we note that every $\simeq$60 kyr the orbital planes get very close to each other. These are the moments when the instantaneous collision probability with Ceres becomes even larger than the average stated above. Obviously, in order for a close encounter to really happen, Ceres must be close to its aphelion and Veritas member close to its perihelion. The difference in g frequencies is much larger than in s frequencies, so the time-scale of very favourable collision probability of Veritas members to Ceres is $\simeq$60 × (360/5) kyr or $\simeq$4 Myr (assuming, for simplicity, that in the Ceres orbital plane the orbit of Veritas members must be oriented within $\simeq 5^\circ$ with respect to the optimum aphelion–perihelion configuration). Therefore, during the estimated age of Veritas family, a typical member may undergo up to three such close encounters to Ceres. This is consistent with data in the top and right-hand panel of Fig. 13. Note that the additional nodal drift of (1086) Nata underwent two changes of rate at approximately 3 Myr and again at about 6.5 Myr.

Obviously, none of the currently observed Veritas members impacted Ceres during its lifetime. We may, however, estimate an order of magnitude of its closest approach $R_{\rm app}$. Considering again the Öpik theory approach, the condition for $R_{\rm app}$ reads: $p_{\rm i} R_{\rm app}^2 T \simeq 1$, where $T = 8.3$ Myr the age of the family. Using this relation we obtain $R_{\rm app} \simeq 5.6 \times 10^5$ km. This result is averaged over all possible orbit configurations. Assuming special coplanarity and alignment conditions would have a much larger collision probability, we may assume the really closest approaches of Veritas fragments to Ceres that occurred few times in the past had $R_{\rm app} \simeq 10^4$ km.

Finally, we estimate the magnitude of orbital semimajor axis jump δa of Veritas member during such a close encounter with Ceres. Obviously, the result depends on details of the encounter. However, here we are interested in obtaining the order of magnitude result only. Assuming the change in binding energy to the Sun is of the order of magnitude of potential energy in the Ceres gravitational field at the moment of the closest approach, we have $(\Delta a/a) \simeq (M_1/M_0)(a/R_{\rm app})$, where M_0 and M_1 are the masses of the Sun and Ceres and a is semimajor axis of the Veritas fragment. We obtain $\delta a \simeq 7 \times 10^{-5}$ au in one encounter. If two such encounters happen statistically, the accumulated Δa becomes about 10^{-4} au.

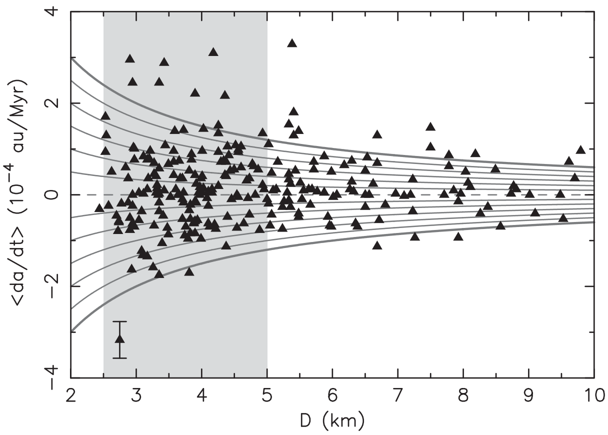

Figure 14. Adjusted semimajor axis drift rates da/dt to achieve optimum convergence in secular angles of 264 $D < 10$ km asteroids in the R_1 region of Veritas family versus their estimated size D. The values correspond to the formal best-fitting solution minimizing χ^2 in Section 5 at 8.23 Myr. The thick grey lines correspond to our estimate of maximum values of the Yarkovsky effect for nominal physical parameters, or $\pm 2.4 \times 10^{-4}$ au Myr^{-1} at $D = 2.5$ km (see Fig. 15) and the characteristic $\propto 1/D$ size dependence. The thin grey lines for respectively smaller da/dt values at the reference size of 2.5 km. The uncertainty interval in da/dt shown for the outlying data point at the bottom left-hand corner applies to all data. This is our estimated realistic value that takes into account: (i) formal variation of da/dt within the sigma interval of the Veritas family age solution (Fig. 8, panel A) and (ii) the stochastic effect of Ceres and Hygiea close encounters on behaviour of the longitude of node and pericentre of asteroids in the Veritas family. The light-grey rectangle indicates the size range 2.5–5 km used for our analysis in Section 5.

To tie this information to our previous results we note that the characteristic accumulated change in semimajor axis of small Veritas members to achieve orbital convergence is $\simeq (5-10) \times 10^{-4}$ au (see Fig. 11). While a part of this value may be due to stochastic effects of Ceres encounters, the main effect is likely due to other dynamical phenomena. We favour the Yarkovsky effect and discuss details in Sections 7 and 8. In this respect, however, the random component due to encounters to Ceres and other massive objects in the belt represents a noise. Given the estimates above, its realistic level is $\simeq 1.3 \times 10^{-5}$ au Myr^{-1} in the mean drift rate due to Ceres along. To stay realistic, we shall assume three times larger value to account for the effects of other massive bodies such as (10) Hygiea.

7 EXPECTED DRIFT RATE IN SEMIMAJOR AXIS DUE TO THE YARKOVSKY EFFECT

For convenience of discussion in this section, we express the empirical accumulated change in semimajor axis in $\simeq$8.23 Myr of the Veritas family age shown in Fig. 11 in terms of the equivalent mean rate. This is shown in Fig. 14. Here we pay attention to the consistency of these values with the predictions from the Yarkovsky effect theory. In particular, we estimate the expected values of the Yarkovsky effect for these bodies and compare them with the empirical values required by orbital convergence discussed in Section 5. A general information about the theory of the Yarkovsky effect may be found in Bottke et al. (2006) or Vokrouhlický et al. (2015). Here we only summarize few facts needed for our application.

While in principle there is only one Yarkovsky effect acting on the body as such, it is customary to divide it into diurnal and seasonal components. Recall that the thermal response of the body surface on solar heating is frequency dependent and there are typically two primary frequencies involved (unless tumbling rotation state that we disregard in this study): (i) rotation frequency ω, and (ii) revolution frequency (or mean motion) n about the Sun. Virtually in all asteroid applications $\omega \gg n$. In this limit, we may consider the thermal effects related to ω (the diurnal component) and those related to n (the seasonal component) frequencies separately. Their mutual interaction is negligible (see e.g. Vokrouhlický 1999). In applications of the Yarkovsky effect to the motion of small asteroids only the diurnal component has been considered so far, while the seasonal component has been neglected. There are two reasons that justified this approach. First, in the limit of very low-enough surface thermal inertia values, appropriate for multikilometre and larger asteroids in the main belt whose surfaces are expected to be covered with fine regolith layer, the magnitude of the seasonal effect becomes $\simeq\sqrt{n/\omega}$ smaller than that of the diurnal effect. Second, the seasonal effect may become important only for a restricted interval of obliquity values near 90°. For evolved-enough populations of asteroids, the Yarkovsky–O'Keefe–Radzievskii–Paddack (YORP) effect makes the obliquity pushed towards the extreme values 0° or 180° (e.g. Bottke et al. 2006 or Vokrouhlický et al. 2015) where the seasonal Yarkovsky effect becomes nil. However, in the case of Veritas fragments, none of these arguments might be satisfied. Thermal inertia of fresh, C-type objects might be anomalously large, compared to the data of all asteroids. At the same time, the YORP effect likely did not have enough time to push the obliquity values of the currently observed Veritas members to their asymptotic values (see also Section 7.1). As a result, we include both the diurnal and the seasonal components of the Yarkovsky effect in our analysis.

Given only the moderate value of the orbital eccentricity of the Veritas family members, we restrict to the Yarkovsky model applicable to circular orbits. This is sufficient, because the eccentricity corrections to the mean orbital change in semimajor axis are only of the second order in e. At the same time, we limit ourselves to the analytic model for the spherical shape of the asteroids and linearized boundary conditions of the heat conduction. While approximate, the main advantage is that we thus dispose of simple analytic formulas for the secular long-term change of the orbital semimajor axis. Finally, we note that the penetration depth ℓ of the thermal wave for both diurnal and seasonal effects is much smaller than the characteristic radius R of the known Veritas members (ℓ being at maximum few metres even for the seasonal effect; e.g. Bottke et al. 2006; Vokrouhlický et al. 2015). In this case, we neglect corrections of the order $\propto\ell/R$ or higher in our analysis.

Using all these approximations, we find that the mean semimajor axis drift rate due to the diurnal variant of the Yarkovsky effect is given by

$$\left(\frac{\mathrm{d}a}{\mathrm{d}t}\right)_{\mathrm{diu}} \simeq \frac{4\alpha}{9}\frac{\Phi}{n}\frac{\Theta}{1+\Theta+\frac{1}{2}\Theta^2}\cos\gamma, \tag{6}$$

where $\alpha = 1 - A$, with A the Bond albedo, $\Phi = (\pi D^2 F)/(4mc)$, with the size (diameter) D of the body, $F \simeq 136.3$ W m^{-2} the solar radiation flux at the mean heliocentric distance of the Veritas family, m the mass of the body, c is the velocity of light and n the orbital mean motion. Note that $\Phi \propto 1/D$, which implies the Yarkovsky effect magnitude is inversely proportional to the asteroid size. Therefore it is negligible for large Veritas members such as (1086) Nata, but becomes important as soon as D becomes smaller than $\simeq$5–10 km. Similarly, denoting ρ asthe bulk density of the asteroid, one has $\Phi \propto 1/\rho$, again the inverse proportional scaling with this parameter. The thermal parameter $\Theta = \Gamma\sqrt{\omega}/(\epsilon\sigma T_\star^3)$ depends on the surface thermal inertia Γ, the rotation frequency ω, the surface infrared emissivity ϵ, the Stefan–Boltzmann constant σ and subsolar temperature $T_\star = [\alpha F/(\epsilon\sigma)]^{1/4}$. Finally, γ is the obliquity of the asteroid spin axis.

Using the same notation as above, the mean semimajor axis drift rate due to the seasonal component of the Yarkovsky effect reads

$$\left(\frac{\mathrm{d}a}{\mathrm{d}t}\right)_{\mathrm{sea}} \simeq -\frac{2\alpha}{9}\frac{\Phi}{n}\frac{\bar{\Theta}}{1+\bar{\Theta}+\frac{1}{2}\bar{\Theta}^2}\sin^2\gamma. \tag{7}$$

This is very similar to equation (6), except for the diurnal thermal parameter Θ now replaced with its seasonal counterpart $\bar{\Theta} = \Gamma\sqrt{n}/(\epsilon\sigma T_\star^3)$. Note that the only difference consists in the rotation frequency ω being substituted with the orbital mean motion n. Thus $\bar{\Theta}$ is always smaller than Θ since $\bar{\Theta}/\Theta = \sqrt{n/\omega}$. Importantly enough, the diurnal and seasonal effects have also different dependence on the rotation pole obliquity γ, the former being maximum at $\gamma = 0°$ and 180°, the latter at $\gamma = 90°$. Hence, the aforementioned YORP-driven depletion of the obliquity distribution at mid-γ values contributes to dominance of the diurnal effect. However, when the YORP effect does not have enough time to modify obliquity values, as we check in the next section, there is no obvious reason to neglect the role of $\gamma \simeq 90°$ obliquity values.

The total rate in semimajor axis is simply $\mathrm{d}a/\mathrm{d}t = (\mathrm{d}a/\mathrm{d}t)_{\mathrm{diu}} + (\mathrm{d}a/\mathrm{d}t)_{\mathrm{sea}}$. For a given body, $\mathrm{d}a/\mathrm{d}t$ depends on a number of physical parameters described above. In some cases the dependence conforms to a simple scaling. Thus, $\mathrm{d}a/\mathrm{d}t \propto \Phi \propto 1/(D\rho)$. For other parameters the dependence is less obvious and needs to be explored numerically. This is the case of the surface thermal inertia Γ, rotation frequency ω and obliquity γ. Obviously, we do not know any of these values for small members in the Veritas family. It is not, however, our intent here to speculate about individual bodies in the Veritas family. Rather, by comparison with the derived $\mathrm{d}a/\mathrm{d}t$ values in Section 5, we may be only able to say something about distribution of these parameters in the whole sample of small Veritas members.

To assist with this goal, we performed the following numerical experiment that may serve as a template for comparison with real Veritas data. Fig. 15 shows results where we fixed a reference asteroid size $D = 2.5$ km, bulk density $\rho = 1.3$ g cm^{-3} and rotation period 6 h (implying thus $\omega \simeq 2.9 \times 10^{-4}$ rad s^{-1}). The chosen size corresponds to that of the smallest Veritas members, for which we were able to determine $\mathrm{d}a/\mathrm{d}t$ value from the secular angles convergence (Fig. 14). The assumed bulk density is the best guess for the C-type taxonomy of the Veritas family (e.g. Scheeres et al. 2015). Two more parameters remain to be selected for predicting the Yarkovsky value of $\mathrm{d}a/\mathrm{d}t$, namely the surface thermal inertia Γ and obliquity γ. For the latter, we assume an isotropic distribution of the spin axes in space. This is, in fact, the underlying hypothesis that we are going to test in comparison with the data. For the former, we assumed a lognormal distribution with two different mean values of 100 SI units (left-hand panel) and 250 SI units (right-hand panel). Both values are within the expected range of thermal inertia values of small, C-type asteroids (fig. 9 of Delbò et al. 2015).

The maximum range of possible $\mathrm{d}a/\mathrm{d}t$ values due to the Yarkovsky effect spans, for the chosen parameters, from about -2.4×10^{-4} to 2.4×10^{-4} au Myr^{-1}. Given the 6 h rotation

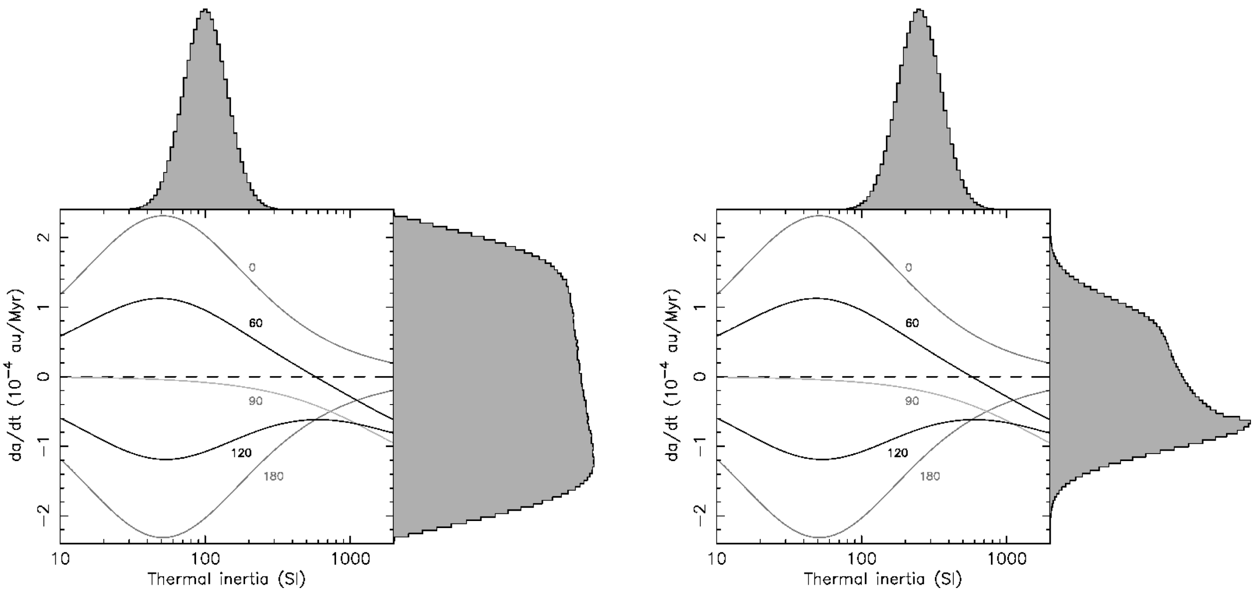

Figure 15. The middle part on the left- and right-hand panels shows dependence of the total semimajor axis drift rate due to the Yarkovsky effect on the surface thermal inertia Γ (we assumed $D = 2.5$ km size member in the Veritas family with a rotation period of 6 h and a bulk density $\rho = 1.3$ g cm^{-3}). Different curves for five representative values of the obliquity $\gamma = 0^\circ$, 60°, 90°, 120° and 180° (labels). Assuming a population of bodies with a lognormal distribution of Γ values shown by the top histograms, and isotropic distribution of spin axis orientations in space, one would obtain distributions of the da/dt values shown on the right-hand side of each of the panels. The difference between left and right is in the mean value of Γ: 100 SI units on the left and 250 SI units on the right.

period it corresponds to 0° or 180° obliquity values and $\Gamma \simeq 50$ in SI units. These limits would be the same for other rotation periods, because the diurnal Yarkovsky effect, the only component contributing at extreme obliquity values, is invariant when Γ and ω change preserving $\Gamma\sqrt{\omega}$ value (see equation 6). So for longer rotation periods the optimum thermal inertia would just slightly shift to the larger values. These maximum values favourably compare with majority of our solved da/dt values for small fragments in the Veritas family (Fig. 14). The few outliers beyond these limits, may be bodies residing on slightly unstable orbits for which our analysis is not so accurate (for instance due to close encounters to Ceres or Hygiea, or secular effects due to these massive bodies in the main belt). Alternately, these cases may also correspond to anomalously low-density fragments, or bodies for which the absolute magnitude has not been determined accurately and they actually have quite smaller size.

The Yarkovsky effect at 90° obliquity is the pure seasonal contribution. At low Γ values this component is basically nil, but at $\Gamma \simeq 700$ in SI units it rivals the maximum value of the diurnal effect. At still reasonable Γ values between 300 and 400 in SI units its contribution is not negligible and needs to be taken into account. The contribution of the seasonal effect makes the total Yarkovsky da/dt value at generic obliquities, such as 60° or 120° on Fig. 15, bent towards negative values for sufficiently large thermal inertia, breaking thus the symmetry between the positive and negative da/dt values.

Let us assume a population of Veritas fragments with an isotropic distribution of spin axes and lognormal tight distributions of Γ values shown by the top histograms in the left- and right-hand panels of Fig. 15. The histograms along the right ordinate then indicate what would be the distribution of da/dt values for this sample. As already expected, the contribution of the seasonal Yarkovsky effect makes it that in both cases the negative da/dt values are more likely. However, for low thermal inertia values (left-hand panel), the asymmetry is only small, 52.4 per cent versus 47.6 per cent of all cases only. This asymmetry becomes more pronounced for larger thermal inertia values (right-hand panel), for which 59.2 per cent cases have da/dt negative and only 40.8 per cent cases have da/dt positive. Playing with more assumptions about the thermal inertia distributions one may thus create other templates for the da/dt distributions for samples of fragments that have their spin axes isotropically distributed in space.

Obviously, if none of such templates corresponds to the observed distribution of da/dt values in the Veritas family, the underlying assumption of isotropy of the rotation axes must be violated. With only limited data, and a lack of information about fragments of other physical parameters, we cannot solve for the spin axis distribution, but at least say some trends. This is the goal of our analysis in Section 7.1.

7.1 A possible role of the YORP effect?

Before we proceed with comparison of the observed and modelled da/dt values, we pay a brief attention to the neglected role of the YORP effect. In particular, we assumed that the $\simeq$8.3 Myr age of the Veritas family is short enough that the YORP toques did not result in a significant change of obliquity γ of its members (such that γ could be considered constant in our analysis). This may look odd at the first sight, because the Yarkovsky and YORP effects are just two faces of one physical phenomenon, namely the recoil effect of thermally re-radiated sunlight by the asteroid surface.

The key element in understanding this issue is a different dependence on the size D. While the Yarkovsky effect is only inversely proportional to D (da/d$t \propto 1/D$, see above), the YORP effect is inversely proportional to D^2. As a result, its importance decreases much faster with increasing size of the bodies.

The model predictions of the YORP effect are much less certain than those of the Yarkovsky effect (see e.g. discussion in Vokrouhlický et al. 2015). In this situation we rather use real data from the Karin family (Carruba et al. 2016), and re-scale them to the case of the Veritas family. This simple re-scaling procedure

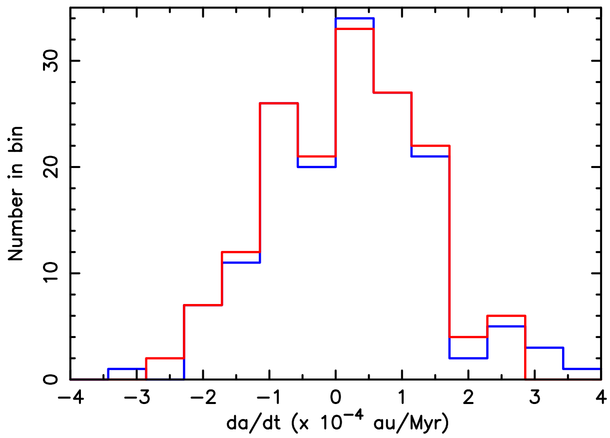

Figure 16. Result of a formal fit of the observed da/dt values for 160 Veritas members with estimated size ≤5 km all mapped to a reference size of 2.5 km using the $\propto 1/D$ scaling (blue histogram). The bin width, $\simeq 0.6 \times 10^{-4}$ au Myr^{-1}, is only slightly smaller than the estimated realistic uncertainty of the da/dt values of individual asteroids because of the effect of massive bodies in the main belt. The red histogram is a best fit from a simulation, where we assumed (i) isotropic distribution of rotation poles, (ii) rotation period 7 h, (iii) mean surface thermal inertia 158 in SI units and (iv) bulk density 1.07 g cm^{-3}.

must take into account different heliocentric distances ($a \simeq 2.86$ au versus $a \simeq 3.16$ au), bulk densities ($\rho \simeq 2.5$ g cm^{-3} versus $\rho \simeq 1.3$ g cm^{-3}) and ages ($T \simeq 5.8$ Myr versus $T \simeq 8.3$ Myr). The accumulated change $\Delta\gamma$ in obliquity scales with $\propto T/(\rho a^2 D^2)$. This makes us to conclude that $D \simeq 2$ km Karin asteroids should accumulate about the same obliquity change as $D \simeq 3$ km Veritas asteroids (the smaller bulk density and larger age playing the main role). Looking at fig. 5 of Carruba et al. (2016), we conclude that the YORP effect is negligible for those sizes (as it has been also verified in that paper). Since $D \simeq 3$ km are about the smallest asteroids we presently observe in the Veritas family, the omission of the YORP effect in this study is justified. For the sake of comparison we note that the population of $D \simeq 1.4$ km Karin asteroids already revealed traces of the YORP effect (fig. 5 in Carruba et al. 2016). Therefore we predict that, when the future observations will allow to discover $D \simeq 2$ km members in the Veritas family, we should start seeing similar YORP pattern as in the Karin family (i.e. depletion of the da/d$t \simeq 0$ values).

8 COMPARISON OF THE OBSERVED AND MODELLED YARKOVSKY DRIFT VALUES

Here we describe the sample of the solved-for values of the Yarkovsky drift da/dt from Section 5 in some detail. However, the reader is to be warned upfront that we show here just an example of many possible solutions. The data are simply not constraining the model enough at this moment.

We already observed the overall consistency of the maximum determined da/dt with the Yarkovsky prediction for the sizes of Veritas members. Here we consider a subsample of 190 asteroids with size $D \leq 5$ km. This is because data for small enough asteroids should enable a better description of the Yarkovsky effect and be less contaminated in a relative sense by the perturbation from Ceres and massive asteroids. We use the inverse-proportional relation between da/dt and D and map all these values to the reference size $D_{\rm ref} = 2.5$ km. This corresponds to the smallest observed Veritas members (Fig. 14). The blue histogram in Fig. 16 shows distribution of these mapped values. We used $\simeq 0.6 \times 10^{-4}$ au Myr^{-1} width of the bins for two reasons: (i) the number of asteroids in the sample is not very large and (ii) the realistic uncertainty of the individual da/dt solutions is $\simeq \pm 0.4 \times 10^{-4}$ au Myr^{-1}, only slightly larger than the bin. The latter is mainly due to the stochastic effect of close encounters with Ceres and Hygiea (Section 6). Therefore it does not make sense to use smaller bin size. There are 95 objects with da/d$t > 0$, and only 65 with da/d$t < 0$, in our sample. At the first sight, this precludes a possibility of isotropic distribution of spin axes (see discussion in Section 7). However, we demonstrate below that the small statistics of bodies still allows matching the data with the underlying pole isotropy. Obviously, solutions with anisotropic pole distribution are also possible, but these are not attempted here, because they would involve many more unconstrained degrees of freedom in the model.

We conducted the following simple numerical experiment. Considering 160 $D = D_{\rm ref} = 2.5$ km size members of the Veritas family, we randomly sampled a three-dimensional parametric space of (i) characteristic rotation period P values (given the same to all bodies), (ii) mean surface thermal conductivity $\bar{\Gamma}$ with a tight lognormal distribution with standard deviation of 0.1 in log Γ (see the top histograms on Fig. 15) and (iii) bulk density ρ. The tested interval of values were (i) 4–20 h for P, (ii) 50–1000 in SI units for $\bar{\Gamma}$ and (iii) 0.8–1.5 g cm^{-3} for ρ. We performed 25 000 trials of a random sampling of this parametric space. For each these choices, we then let the code test 10^4 random variants of spin axes obliquities. Altogether, we thus ran 2.5×10^8 simulations. In each of them we computed the distribution of da/dt values for the sample using equations (6) and (7). We evaluated the formal $\chi^2 = \sum (N_{\rm c} - N_{\rm o})^2$ measure of the difference between the data $N_{\rm o}$ and the model $N_{\rm c}$ using the bins shown in Fig. 16. In particular, we considered only the 10 central bins around zero up to da/dt values of $\pm 2.5 \times 10^{-4}$ au Myr^{-1}, because these are maximum expected Yarkovsky values (e.g. Fig. 15). The solution is largely degenerate, since many parameter combinations resulted in reasonable fits, so we restrict here to summarize just the main trends. These are best shown by a projection of the χ^2 values on to the plane of surface thermal inertia $\bar{\Gamma}$ and bulk density ρ (Fig. 17).

We note that the reasonable matches required (i) $\bar{\Gamma}$ smaller than $\simeq 400$ SI units, and most often being in the interval between 150 and 250, (ii) rotation period values P are not constrained (thus not shown in the Fig. 17) and (iii) the density ρ should be smaller than 1.3 g cm^{-3}. The reason for (i) is explained in Section 7: larger thermal conductivity would necessarily prefer negative values of da/dt that is not observed in our data. Actually the predominance of the positive da/dt is achieved only as a result of statistical noise on low number of data in the individual bins. The low densities are required to match the observed minimum to maximum range of da/dt values.

9 CONCLUSIONS

Our results can be summarized as follows.

(i) We identified and studied the members of the Veritas family and asteroids in the family background. As in Tsiganis et al. (2007), we found that the chaotic orbits with Lyapunov times $<10^5$ yr are in the 3+3-2 and 5-2-2 three-body resonances. (490) Veritas itself is currently in the 5-2-2 resonance and is characterized by a very short Lyapunov time. With a possible exception of the $g - g_{\rm Hygiea}$ secular resonance, secular dynamics plays only a minor role in the region of the Veritas family.

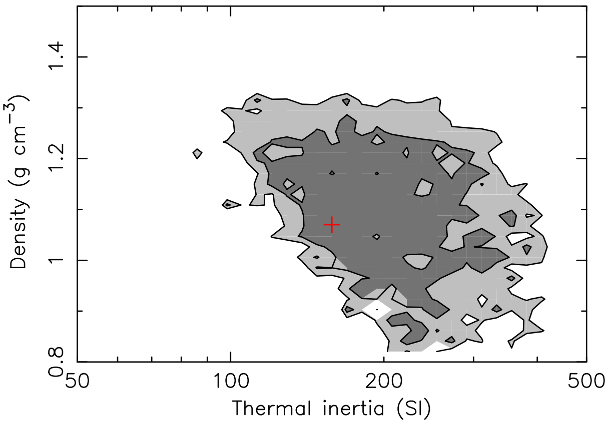

Figure 17. Region of admissible χ^2 values in the parametric space surface thermal inertia $\bar{\Gamma}$ (abscissa) and bulk density ρ (ordinate) of the Veritas family members. The χ^2 is a measure of a success to match distribution of the Yarkovsky rate of change of the semimajor axis $\mathrm{d}a/\mathrm{d}t$ obtained for 160 $D \leq 5$ km asteroids in the R_1 region of the family (see the text). At each grid point in the plane we also tested rotation periods between 4 and 20 h and we run 10^4 trials of isotropically distributed spin axes of the fragments. The light grey area shows where $\chi^2 \leq 40$, the dark grey area shows where $\chi^2 \leq 30$. The formally best-fitting value $\chi^2 = 13$, shown by red cross, corresponds to $\bar{\Gamma} = 158$ (SI units), $\rho = 1.07$ g cm^{-3} and $P = 7$ h (see Fig. 16).

(ii) We studied physical properties of asteroids in the Veritas family region. The Veritas family is mostly made of C-type objects of low albedo. The mean albedo value of the Veritas family is 0.07. Among Veritas members, only (490) Veritas and (1086) Nata have masses larger than 10^{17} kg. The mass distribution of the family is consistent with the outcome of a fragmentation event.

(iii) We investigated the past convergence of nodal longitudes of members of the Veritas family with Lyapunov times $>3 \times 10^4$ yr and refined the list of secure Veritas family members. 704 asteroids have their nodal longitude converging to within $\pm 60^\circ$ to that of (1086) Nata between 8.1 and 8.5 Myr ago.

(iv) By performing two sets of numerical integrations with the Yarkovsky force, we found that the inclusion of the Yarkovsky effect is crucial for improving the convergence. The convergence of nodal longitudes of 274 most regular members of the Veritas family is almost ideal. The best age estimate is $8.23^{+0.37}_{-0.31}$ Myr.

(v) For the first time, we were able to demonstrate the possibility of convergence of the perihelion longitudes. Regrettably, the effect of close encounters with Ceres and other massive main belt asteroids destroys the convergence in ϖ, and also defocuses the convergence of Ω. This limits the accuracy of our Yarkovsky drift estimates to $\pm 4 \times 10^{-5}$ au Myr^{-1}.

(vi) To within this precision, we were able to obtain $\mathrm{d}a/\mathrm{d}t$ drift rates for 274 members of the Veritas family. The drift rates are larger for smaller asteroids, as expected from the Yarkovsky effect. The inferred distribution of $\mathrm{d}a/\mathrm{d}t$ values is consistent with a population of objects with low densities and low thermal conductivities.

(vii) The effects of YORP cannot be discerned in the Veritas family. They should become apparent when future observations will help to characterize the family members with $D < 2$ km.

In summary, despite the very complex dynamical environment of the Veritas family, we were able to refine the family age estimate, obtain Yarkovsky drift rates for 274 family members and constrain several key parameters such as their bulk density and thermal conductivity. Results are consistent with the standard theory of the Yarkovsky effect.

ACKNOWLEDGEMENTS

We are grateful to the reviewer of this paper, Professor Andrea Milani, for comments and suggestions that significantly improved the quality of this work. We would like to thank the São Paulo State Science Foundation (FAPESP) that supported this work via the grant 16/04476-8, and the Brazilian National Research Council (CNPq, grant 305453/2011-4). VC was a visiting scientist at the Southwest Research Institute (SWRI) during the preparation of this paper. DV's work was funded by the Czech Science Foundation through the grant GA13-01308S. DN's work was supported by the NASA Solar System Workings program. This publication makes use of data products from the *Wide-field Infrared Survey Explorer* (*WISE*) and *Near-Earth Object Wide-field Infrared Survey Explorer* (*NEOWISE*), which are a joint project of the University of California, Los Angeles, and the Jet Propulsion Laboratory/California Institute of Technology, funded by the National Aeronautics and Space Administration.

REFERENCES

Bendjoya P., Zappalà V., 2002, in Bottke W. F., Jr, Cellino A., Paolicchi P., Binzel R. P., eds, Asteroid III. Univ. Arizona Press, Tucson, AZ, p. 613
Bottke W. F., Nolan M. C., Kolvoord R. A., Greenberg R., 1994, Icarus, 107, 255
Bottke W. F., Vokrouhlický D., Rubincam D. P., Brož M., 2002, in Bottke W. F. Jr, Cellino A., Paolicchi P., Binzel R. P., eds, Asteroid III. Univ. Arizona Press, Tucson, AZ, p. 395
Bottke W. F., Vokrouhlický D., Rubincam D. P., Nesvorný D., 2006, Annu. Rev. Earth Planet. Sci., 34, 157
Brož M., 1999, Thesis, Charles Univ., Prague, Czech Republic
Brož M., Morbidelli A., Bottke W. F., Rozehnal J., Vokrouhlický D., Nesvorný D., 2013, A&A, 551, A117
Carruba V., 2010, MNRAS, 408, 580
Carruba V., 2013, MNRAS, 431, 3557
Carruba V., Nesvorný D., 2016, MNRAS, 457, 1332
Carruba V., Burns J. A., Bottke W., Nesvorný D., 2003, Icarus, 162, 308
Carruba V., Huaman M., Douwens S., Domingos R. C., 2012, A&A, 543, A105
Carruba V., Huaman M., Domingos R. C., Roig F., 2013, A&A, 550, A85
Carruba V., Domingos R. C., Huaman M., Dos Santos C. R., Souami D., 2014, MNRAS, 437, 2279
Carruba V., Nesvorný D., Vokrouhlický D., 2016, AJ, 151, 164
Delbò M., Mueller M., Emery J. P., Rozitis B., Capria M. T., 2015, in Michel P., DeMeo F. E., Bottke W. F., eds, Asteroids IV. Univ. Arizona Press, Tucson, AZ, p. 107
DeMeo F. E., Carry B., 2013, Icarus, 226, 723
Farley K. A., Vokrouhlický D., Bottke W. F., Nesvorný D., 2006, Nature, 439, 295
Ivezić Ž. et al., 2001, AJ, 122, 2749
Knežević Z., Milani A., 2003, A&A, 403, 1165
Levison H. F., Duncan M. J., 1994, Icarus, 108, 18
Masiero J. R., Mainzer A. K., Grav T., Bauer J. M., Jedicke R., 2012, ApJ, 759, 14
Michel P., Jutzi M., Richardson D. C., Benz W., 2011, Icarus, 211, 535
Milani A., Farinella P., 1994, Nature, 370, 40
Milani A., Knežević Z., 1994, Icarus, 107, 219
Murray C. D., Dermott S. F., 1999, Solar System Dynamics. Cambridge Univ. Press, Cambridge
Nesvorný D., Bottke W. F., 2004, Icarus, 170, 324
Nesvorný D., Bottke W. F., Levison H. F., Dones L., 2003, ApJ, 591, 486
Nesvorný D., Brož M., Carruba V., 2015, in Michel P., DeMeo F. E., Bottke W. F., eds, Asteroid IV. Univ. Arizona Press, Tucson, AZ, p. 297
Scheeres D. J., Britt D., Carry B., Holsapple K. A., 2015, in Michel P., DeMeo F. E., Bottke W. F., eds, Asteroids IV. Univ. Arizona Press, Tucson, AZ, p. 745

Tsiganis K., Knežević Z., Varvoglis H., 2007, Icarus, 186, 484
Vokrouhlický D., 1999, A&A, 334, 362
Vokrouhlický D., Bottke W. F., Chesley S. R., Scheeres D. J., Statler T. S., 2015, in Michel P., DeMeo F. E., Bottke W. F., eds, Asteroids IV. Univ. Arizona Press, Tucson, AZ, p. 509

SUPPORTING INFORMATION

Supplementary data are available at *MNRAS* online.

Table B1. Proper elements and estimated drift rates of 274 Veritas family members.
MR_table.txt

Please note: Oxford University Press is not responsible for the content or functionality of any supporting materials supplied by the authors. Any queries (other than missing material) should be directed to the corresponding author for the paper.

APPENDIX A: PROPER FREQUENCY BEHAVIOUR IN THE VERITAS REGION

Following the approach of Nesvorný & Bottke (2004) we attempt to compute the drift rates caused by the Yarkovsky effect based on the values of $\Delta\Omega$, the difference between the values of Ω between those of the 705 members of the Veritas family and those of (1086) Nata itself. For this purpose, we first need to determine how the g and s proper frequencies depend on proper semimajor axis in the Veritas region. Contrary to the case of the Karin cluster, we cannot use for the Veritas family the convergence of the past longitudes of the nodes ϖ, since the Veritas family is too close to the 2/1 mean-motion resonance with Jupiter, and this causes the precession of the longitude of the nodes to increase significantly. According to Nesvorný & Bottke (2004), values of $\Delta\Omega_{\mathrm{P},j}$ for a given j member at each given time $t = -(\tau + \Delta t)$, with τ the estimated age of the Karin group, is given by

$$\Delta\Omega_{\mathrm{P},j}(t) = \Omega^*_{\mathrm{P},j} - \Omega^*_{\mathrm{P},1} - \frac{1}{2}\frac{\partial s}{\partial a_{\mathrm{P}}}(\delta a_{\mathrm{P},j} - \Delta a_{\mathrm{P},1})\tau - (s_j - s_1)\Delta t, \quad \text{(A1)}$$

where $\Omega^*_{\mathrm{P},j} - \Omega^*_{\mathrm{P},1}$ is the proper nodal longitude difference caused by the ejection speeds ΔV, and assumed negligible hereafter (Nesvorný & Bottke 2004 estimate that it is of the order of 1° for the Karin cluster, and should not be much larger for the Veritas family). $\frac{\partial s}{\partial a_{\mathrm{P}}}$ define how frequencies change with a_{P}. Nesvorný & Bottke (2004) used the analytic perturbation theory of Milani & Knežević (1994) to estimate this rate equal to -70.0 arcsec yr^{-1} au^{-1} for all Karin cluster members (with an uncertainty of 1 per cent caused by the spread in proper a_{P} of the cluster members). The case of the Veritas family is, however, much more challenging.

Fig. A1 displays an (a, s) projection of members of the Karin cluster (panel A) and of the Veritas family (panel B). While indeed most Karin members follow a single line of constant $\delta s/\delta a$ in the (a, s) plane, the distribution of (a, s) for the Veritas family is much more disperse. The local three-body resonances play an important role in affecting the values of asteroid proper in the region of the Veritas family, in a way not observed for the Karin cluster. To investigate the role of the local dynamics, we first obtained a dynamical map of synthetic proper elements in the $(a, \sin i)$ domain.

For this purpose, we created a grid of 1600 particles divided in 40 equally spaced intervals in both osculating a and i and integrated them over 12 Myr over the influence of the Sun and the eight planets with SWIFT_MVSF, the symplectic integrator based on SWIFT_MVS from the SWIFT package of Levison & Duncan (1994), and modified by Brož (1999) to include online filtering of osculating elements. The initial osculating elements of the particles went from 3.150 to 3.190 au in a and from 7°.0 to 11°.0 in i. The other orbital elements of the test particles were set equal to those of (1086) Nata at the Modified Julian Date of 57200. The step in osculating a, 0.001 au, was chosen small enough to allow for a significant resolution in the map, but large enough so that the computation of $\delta s/\delta a$ and $\delta g/\delta a$ was precise enough, considering the errors in proper frequencies and semimajor axis. Synthetic proper elements were then obtained with the approach described in Carruba (2010), based on the method of Knežević & Milani (2003).

Results are shown in Fig. A2, panel (A). Black dots display the location of the test particles synthetic proper elements. Not surprisingly, one can notice (i) the important perturbing effect of the 5-2-2 resonance, and (ii) the absence of important secular resonances in this region, apart from the $\nu_{1H} = g - g_{\mathrm{Hygiea}}$ located at $\simeq$3.170 au (not shown in the figure for simplicity), that further contributes to the chaotic dynamics between the 3+3-2 and 5-2-2 three-body resonances. Based on the values of proper frequencies g and s obtained

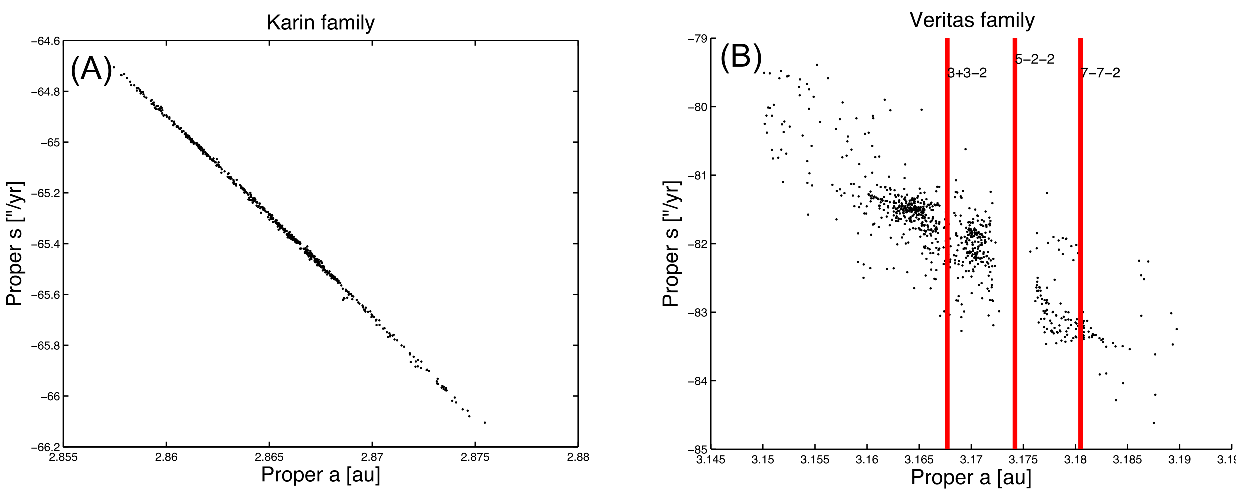

Figure A1. An (a, s) projection of members of the Karin cluster (panel A) and of the Veritas family (panel B). While the (a, s) distribution of the Karin cluster members mostly follows a single line of constant $\delta s/\delta a$, the same distribution for the Veritas family is much more dispersed.

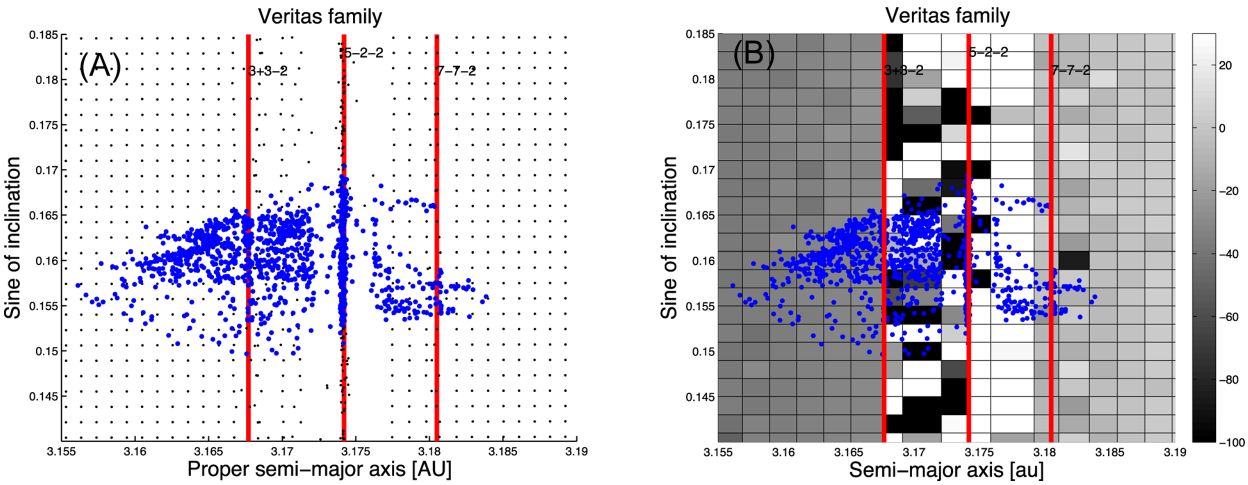

Figure A2. An (a, sin i) dynamical map of the region of the Veritas family (panel A). Black dots identify the values of synthetic proper elements of the integrated test particles. Other symbols are the same as in Fig. 1. Panel (B) displays a colour plot of values of $\delta s/\delta a$ obtained for the particles in the dynamical map simulation.

Table B1. Proper elements and estimated drift rates of 274 Veritas family members.

Number	H	a_P (au)	e_P	sin i_P	g_P (arcsec yr^{-1})	s_P (arcsec yr^{-1})	LCE × 10^6 (yr^{-1})	Drift speed (au Myr^{-1})
1086	9.49	3.165357	0.061441	0.161970	127.944574	−81.597922	1.45	0.000E+00
6374	11.95	3.165615	0.061238	0.161059	128.412635	−81.663237	1.34	−0.800E-04
7231	12.14	3.165802	0.061364	0.160469	128.750656	−81.730850	0.33	−0.220E-03
8624	13.55	3.164742	0.061074	0.162768	127.137085	−81.472127	1.47	0.800E-03
9715	13.23	3.165485	0.060828	0.159609	128.625973	−81.736346	1.87	−0.740E-03
9860	13.07	3.164893	0.060683	0.161880	127.484952	−81.514396	1.46	−0.140E-03
11768	12.93	3.164016	0.060272	0.162164	126.564674	−81.416291	1.50	0.300E-03
15066	12.23	3.165616	0.061469	0.162364	128.100351	−81.579624	1.38	−0.240E-03
15256	12.52	3.164626	0.060472	0.161926	127.209465	−81.479886	1.52	0.820E-03
15732	12.38	3.164794	0.060991	0.162029	127.366566	−81.526495	1.40	0.999E-04

for this map, we then computed the values of $\delta g/\delta a$ and $\delta s/\delta a$ with this method: for each point in the line of 40 intervals in a in the map, with the exception of the first and last, we computed the distance in proper a, da, and in proper frequencies dg and ds of the neighbour to the left with respect to the neighbour to the right. $\delta g/\delta a$ and $\delta s/\delta a$ were then assumed equal to dg/da and ds/da, respectively. Results shown in Fig. A2, panel (B) display a colour plot of our results for $\delta s/\delta a$ (results for $\delta g/\delta a$ are analogous and will not be shown, for simplicity). For semimajor axis lower than those of the centre of the 3+3-2 resonance the behaviour of $\delta s/\delta a$ is quite regular, slowly increasing with respect to a. $\delta s/\delta a$ becomes much more erratic between the 3+3-2 and 5-2-2 resonances, and only returns to a more regular behaviour for values of semimajor axis larger than 3.18 au, beyond the locations of the 5-2-2 and the 7-7-2 three-body resonances. In view of the complex behaviour observed for $\delta s/\delta a$ and $\delta g/\delta a$, we decided not to use an analytic approach to obtain family ages and drift rates based on these values.

APPENDIX B: YARKOVSKY DRIFT SPEED VALUES

We report in Table B1 the first 10 identified Veritas members, their absolute magnitude, proper $a, e, \sin i, g$ and s, Lyapunov exponent (multiplied by a factor 10^6) and estimated mean Yarkovsky drift speed, in au Myr^{-1} [no such value is available for (1086) Nata itself because of its relative large size has very limited Yarkovsky mobility). The complete table for the whole sample of 274 studied asteroids is available in the online version of this paper.

This paper has been typeset from a TEX/LATEX file prepared by the author.